THE JOURNAL OF BIOLOGICAL CHEMISTRY VOL. 290, NO. 7, pp. 4248–4259, February 13, 2015

A Sorting Signal Suppresses IFITM1 Restriction of Viral Entry*

Received for publication, December 5, 2014 Published, JBC Papers in Press, December 19, 2014, DOI 10.1074/jbc.M114.630780

Kun Li[‡1], Rui Jia[§2,3], Minghua Li[‡2], Yi-Min Zheng[‡], Chunhui Miao[‡], Yunfang Yao[§], Hong-Long Ji[¶], Yunqi Geng[§], Wentao Qiao[§], Lorraine M. Albritton[‖4], Chen Liang[‡‡4], and Shan-Lu Liu[‡5]**

*From the [‡]Department of Molecular Microbiology and Immunology, Bond Life Sciences Center, University of Missouri, Columbia, Missouri 65211, the [§]Key Laboratory of Molecular Microbiology and Biotechnology (Ministry of Education) and Key Laboratory of Microbial Functional Genomics (Tianjin), College of Life Sciences, Nankai University, Tianjin 300071, China, the [¶]Department of Cellular and Molecular Biology, Texas Lung Injury Institute, University of Texas Health Science Center, Tyler, Texas 75708, the [‖]Department of Microbiology, Immunology, and Biochemistry, University of Tennessee Health Science Center, Memphis, Tennessee 38163, the **McGill AIDS Centre, Lady Davis Institute, Montreal, Quebec H3T 1E2, Canada, and the [‡‡]Department of Microbiology and Immunology, McGill University, Montreal, Quebec H3A 2B4, Canada*

Background: IFITM1 differentially inhibits viral entry.
Results: IFITM1 associates with AP-3; mutation of the C-terminal KR*XX* motif of IFITM1 results in loss of AP-3 interaction yet increases viral entry.
Conclusion: KR*XX* is a potential sorting motif targeting IFITM1 to lysosome.
Significance: Our results provide new insight into the mechanism of IFITM1 restriction of viral infection.

The interferon-induced transmembrane proteins (IFITMs) broadly inhibit virus infections, particularly at the viral entry level. However, despite this shared ability to inhibit fusion, IFITMs differ in the potency and breadth of viruses restricted, an anomaly that is not fully understood. Here, we show that differences in the range of viruses restricted by IFITM1 are regulated by a C-terminal non-canonical dibasic sorting signal KR*XX* that suppresses restriction of some viruses by governing its intracellular distribution. Replacing the two basic residues with alanine (KR/AA) increased restriction of jaagsiekte sheep retrovirus and 10A1 amphotropic murine leukemia virus. Deconvolution microscopy revealed an altered subcellular distribution for KR/AA, with fewer molecules in LAMP1-positive lysosomes balanced by increased levels in CD63-positive multivesicular bodies, where jaagsiekte sheep retrovirus pseudovirions are colocalized. IFITM1 binds to cellular adaptor protein complex 3 (AP-3), an association that is lost when the dibasic motif is altered. Although knockdown of AP-3 itself decreases some virus entry, expression of parental IFITM1, but not its KR/AA mutant, potentiates inhibition of viral infections in AP-3 knockdown cells. By using the substituted cysteine accessibility method, we provide evidence that IFITM1 adopts more than one membrane topology co-existing in cellular membranes. Because the C-terminal dibasic sorting signal is unique to human IFITM1, our results provide novel insight into understanding the species- and virus-specific antiviral effect of IFITMs.

Interferon (IFN) is a potent immune mediator produced by cells in response to pathogen invasion, especially viral infections. IFN-stimulated genes interfere with and modulate various stages of the viral replication cycles (1). The IFN-induced transmembrane proteins (IFITMs)[6] comprise a group of small IFN-stimulated genes that have been shown to inhibit the early stages of virus replication, particularly the entry step (2, 3). Humans express at least four IFITMs: IFITM1, -2, and -3 are ubiquitously expressed, whereas IFITM5 is limited to osteoblasts (4). Cells and tissues normally express basal levels of IFITMs that are substantially increased by IFN or upon virus infection (4). Currently, the mechanism by which IFITMs inhibit viral infection remains elusive.

Genetic screens using IFITM-specific small interfering RNA identified human IFITM1, -2, and -3 as potent inhibitors of infection by influenza A virus (IAV), West Nile virus, and dengue virus (5). Subsequent work from a number of groups, including us, showed that human IFITMs as well as those of other species restrict Marburg virus, Ebola virus, SARS coronavirus, vesicular stomatitis virus (VSV), jaagsiekte sheep retrovirus (JSRV), and human immunodeficiency virus type 1 (HIV-1) (6–11). More recently, additional viruses, including some non-enveloped viruses, have also been shown to be restricted by IFITMs (12, 13). *In vivo*, IFITM3 strongly limits the morbidity and mortality of IAV infection in mice and humans; a splice site mutation resulting in deletion of the first 21 amino acids of IFITM3 has been found to be associated with more severe disease and hospitalization in the 2009 H1N1 influenza pandemic

* This work was supported, in whole or in part, by National Institutes of Health Grants AI 105584, AI 112381, and AI 109464 (to S. L. L.). This work was also supported by Canadian Institutes of Health Research Grant MOP-77649 (to C. L. and S. L. L.).
[1] Present address: Dept. of Pediatrics, University of Iowa, Iowa City, IA 52240.
[2] Both authors contributed equally to this work.
[3] Present address: Cell Biology and Metabolism Branch, NICHD, National Institutes of Health, Bethesda, MD 20892.
[4] Both authors contributed equally to this work.
[5] To whom correspondence should be addressed: Dept. of Molecular Microbiology and Immunology, Bond Life Sciences Center, University of Missouri, Columbia, MO 65211. Tel.: 573-882-440; Fax: 573-884-9395; E-mail: liushan@missouri.edu.

[6] The abbreviations used are: IFITM, interferon-induced transmembrane protein; JSRV, jaagsiekte sheep retrovirus; MLV, murine leukemia virus; IAV, influenza A virus; MSD, membrane-spanning domain; MVBs, multivesicular bodies; AP, adaptor protein complex; HTX, a subclone of HT1080; 293/GP-LAPSN, a 293 packaging cell line expressing MLV Gag-Pol and alkaline phosphatase; 293/LH2SN, 293 cells overexpressing JSRV receptor Hyal2; SCAM, substituted cysteine accessibility method; mPEG, maleimide polyethyleneglycol; VSV, vesicular stomatitis virus; Env, envelope; 4KR, mutant in which all four conserved lysines are replaced by arginine; KR/AA, mutant in which two basic residues Lys and Arg are replaced with alanine.

(14, 15), although some controversies need to be resolved (16, 17).

Although it has been shown that IFITMs inhibit viral entry, the exact mechanisms by which this is accomplished are poorly understood (18–22). We recently reported evidence that IFITMs inhibit membrane fusion of all three classes of viral fusion proteins, which explains, at least in part, the broad antiviral effects of these proteins (11). We showed that IFITMs do not interfere with specific receptor binding or low pH-mediated triggering but that the creation of membrane hemifusion, a requisite intermediate in biological membrane fusion, is blocked by IFITMs (11). Our results are consistent with two other reports, one showing that IFITM3 protein interacts with vesicle membrane protein-associated protein A and disrupts intracellular cholesterol homeostasis, thereby blocking viral entry (23, 24). Evidence that IFITMs block other steps of membrane fusion, including pore formation, has also been reported recently (25).

Several lines of evidence suggest that the potency of IFITMs against virus entry is modulated by factors other than their intrinsic ability to inhibit membrane fusion (2, 3). Notably, the degree of potency of IFITMs against viral glycoprotein-mediated membrane fusion does not uniformly manifest in terms of potency against virus infection (11). For example, we showed that whereas IFITM1 and IFITM3 are much more potent than IFITM2 in inhibiting cell-cell fusion induced by IAV hemagglutinin (HA), VSV glycoprotein, and JSRV envelope (Env), these three human IFITMs are almost equally efficient at inhibiting IAV and VSV infection, and IFITM1 has a greater reduction in JSRV infection than IFITM2 and -3 (6, 11). Similarly, despite strong and sometimes profound inhibition of the replication of hepatitis C virus and human immunodeficiency virus 1 (HIV-1), the effect of IFITM1 on hepatitis C virus and HIV-1 entry appears to be modest (8, 26–28). More recently, it was reported that IFITM2 and -3, but not IFITM1, restrict Rift Valley fever virus entry (12) and even enhance a human coronavirus, HCoV-OC43 (29).

Here, we report evidence that the C-terminal sequence of IFITM1 is responsible for differential restriction of JSRV and IAV. This analysis fortuitously revealed two basic residues whose removal from IFITM1 increased its restriction of JSRV and amphotropic murine leukemia virus (MLV). We show that IFITM1 associates with cellular adaptor protein complex 3 (AP-3) and that these associations are lost when the C-terminal dibasic residues are changed to alanine. This feature is quite different from that of IFITM3, which we have recently shown to specifically interact with AP-2 through its *YXX*Φ sorting motif at the N terminus, thereby modulating endocytic trafficking and antiviral activities (30). Our results support a model in which the C-terminal dibasic residues control the intracellular trafficking and localization of IFITM1, thereby differentially modulating viral entry.

EXPERIMENTAL PROCEDURES

Constructs and Cells—The parental N-terminal FLAG-tagged pQCXIP-IFITM1 and IFITM1 C-terminal deletion mutant constructs were described previously (8, 11). The FLAG-tagged chimeras and point mutants of IFITM1 were created by overlapping PCR, with the resulting products cloned into the pQCXIP retroviral vector (Clontech, Mountain View, CA). All mutations were verified by DNA sequencing. The Rab5-GFP, LAMP1-GFP, and CD63-RFP were kind gifts from Walther Mothes (Yale University, New Haven, CT). The μ1A, μ1B, μ2, μ3A, μ3B, and μ4 plasmids were kindly provided by Juan Bonifacino (National Institutes of Health) and Heike Fölsch (Northwestern University, Chicago, IL). JSRV Env, 10A1 MLV Env, and IAV HA/NA constructs have been described previously (8, 11). HA-tagged ubiquitin constructs were gifts of David Pintel (University of Missouri). Lentiviral vectors encoding shRNA targeting AP-3 were purchased from Sigma.

293T, HTX (a subclone of HT1080), 293T/GFP (stably expressing GFP), 293/LH2SN (stably expressing Hyal2), and 293/GP-LAPSN (expressing MLV Gag-Pol and alkaline phosphatase) cells were described previously (11). All mammalian cells were cultured in Dulbecco's modified Eagle's medium (DMEM) with 10% fetal bovine serum (FBS). Stable cell lines expressing IFITM1 mutants were generated by transduction of cells with pQCXIP retroviral vectors bearing the G glycoprotein of VSV followed by selection with puromycin (1 μg/ml) (Sigma).

Immunoprecipitation and Western Blotting—Cells were washed once with PBS buffer and lysed with buffer containing 150 mM NaCl, 1 mM EDTA, 1% Triton X-100, 0.1% Nonidet P-40, 10% glycerol, and 50 mM Tris-HCl, pH 7.4; 1 mM PMSF and complete miniprotease inhibitor mixture (Roche Applied Science) were added immediately before use. Proteins samples were resolved by SDS-PAGE and transferred to a polyvinylidene difluoride (PVDF) membrane (Bio-Rad). The expression of FLAG-tagged IFITM1 and mutants was detected using an anti-FLAG monoclonal antibody (Sigma). Western blotting was probed with an anti-HA monoclonal antibody (Sigma). Appropriate secondary antibodies conjugated to horseradish peroxidase (HRP; Sigma) were used for chemiluminescent detection of primary antibody-reactive proteins.

Syncytium Formation and Cell-Cell Fusion—The syncytium formation assay was performed as described previously (11, 31). Briefly, 293/LH2SN cells stably expressing the indicated WT or mutant IFITM1 were co-transfected with 2 μg of plasmids encoding JSRV Env, 10A1 MLV Env with R peptide deleted, or IAV HA, along with 0.5 μg of peGFP-N1 (Clontech, Mountain View, CA) by the standard calcium phosphate method. Twenty-four hours post-transfection, cells were treated with either pH 7.5 or pH 5.0 buffer (10 mM HEPES, 10 mM morpholine ethanesulfonic acid (MES) in PBS) for 1 min at 37 °C. Cells were then cultured in full growth medium; syncytia formation was monitored from 10 min to 24 h after treatment. Representative images were captured at ×20 magnification of 6–10 fields/sample using an epifluorescent microscope (Leica Microsystems, Wetzlar, Germany).

For the cell-cell fusion assay, effector 293T cells were co-transfected with plasmids encoding Tet-off and 10A1 Env with R peptide deleted, and target cells were 293FT cells expressing Tet-response element-regulated *Gaussia* luciferase (gift of Marc Johnson, University of Missouri). The fusion activity was quantified by measuring the *Gaussia* luciferase activities in culture medium 24–48 h after coculture (32).

Pseudovirion Production and Infection—GFP-encoding and alkaline phosphatase-encoding Moloney murine leukemia virus pseudovirions were produced as described previously (11, 33). Lentiviral shRNA/AP-3 pseudotypes were generated according to the manufacturer's instructions (Sigma). Appropriate amounts of viral supernatants were used to infect target cells in the presence of 5 μg/ml Polybrene (Sigma). For GFP-encoding pseudoviral infection, we typically used a multiplicity of infection of 0.05 and 0.2 for each viral infection, and infected cells were assessed for GFP expression by flow cytometry at 48 h postinfection. For alkaline phosphatase pseudovirus, cells were stained for alkaline phosphatase-positive foci and were scored at 72 h postinfection using light microscopy.

Immunostaining, Three-dimensional Deconvolution Microscopy, and Colocalization Analysis—HTX cells expressing IFITMs of interest were transfected with plasmids encoding different cellular markers. Thirty-six hours after transfection, cells were washed with PBS and fixed in 4% freshly made paraformaldehyde. Cells were permeabilized with 0.25% Triton X-100 for 5 min at room temperature, blocked with 5% BSA for 30 min, and incubated with an anti-FLAG antibody for 1 h at room temperature. After washing with PBS three times, cells were incubated with TRITC-conjugated secondary antibody (Sigma) for 1 h and stained with DAPI (Sigma) to detect nuclei. *Z*-Stack images were taken using Leica DMI6000 B inverted deconvolution microscope with a $\times$60 oil immersion lens. Deconvolution was carried out using LAS AF three-dimensional blind deconvolution. Images were analyzed, with overlaps between IFITM1 proteins or viral particles and endosomal markers determined by using Fiji ImageJ plugins (National Institutes of Health). Note that this approach is not sensitive to intensities of individual pixels in both channels but computes the area fractions of endosomal pixels containing IFITM1 or viral particles. Typically, $>$15 cells were analyzed for each set, and experiments were repeated 2–3 times, with statistical tests carried out using Prism.

Membrane Topology—The substituted cysteine accessibility method (SCAM) experiment was performed as described previously (34), with minor modifications. Briefly, 293T cells were transfected with plasmids encoding IFITM1 WT or mutants with the indicated residues substituted by a cysteine. Twenty-four hours post-transfection, cells were detached by 5 mM EDTA, washed once with cold PBS, and then washed with cold HCN buffer (50 mM HEPES (pH 7.5), 150 mM NaCl, and 2 mM $CaCl_2$). Cells were divided equally into three tubes. One aliquot was left in HCN buffer alone (non-permeabilized), the second was resuspended in 0.04% digitonin, and the third was resuspended in 0.25% Triton X-100; all three samples were incubated for 20 min at 4 °C. Maleimide polyethyleneglycol (mPEG) (5 kDa) (Sigma) was added to each tube with a final concentration of 2 mM and incubated for an additional 30 min at 4 °C, and the reaction was terminated by adding DTT (20 mM) with incubation for 10 min at 4 °C. Triton X-100 (1% final concentration) was added to each tube to completely lyse the cells, and samples were subjected to SDS-PAGE and Western blotting using a mouse monoclonal anti-FLAG antibody (Sigma).

Statistical Analysis—One-way analysis of variance, with Dunnett's multiple comparison methods, was used to perform all statistical tests. Unless otherwise specified, results from 3–5 independent experiments were used for the analysis.

RESULTS

The C-terminal Tail of IFITM1 Regulates Differential Restriction of Viral Entry—We previously showed that IFITM1 restricts JSRV entry more effectively than IFITM2 and -3 in HTX cells (a subclone of HT1080), yet these three IFITMs are equally efficient at inhibiting IAV entry (11). Given that JSRV and IAV enter host cells by different endocytic pathways (caveolin-associated for JSRV *versus* clathrin-mediated for IAV, although other alternate pathways may also be used) and their membrane fusion is triggered by distinct pH thresholds (pH ~6.5 for JSRV *versus* 5.7 for IAV) (11, 35, 36), we hypothesized that the difference in virus restriction patterns might be due to differences in cellular localizations of IFITM1 controlled by specific endocytic sorting signals. Because IFITMs differ primarily in their N- and C-terminal sequences (Fig. 1*A*), we created reciprocal chimeras in these regions of IFITM1 and IFITM2 (Fig. 1*B*) and quantified their ability to restrict entry of JSRV and IAV. Chimeras containing the C-terminal region of IFITM1 (IFITM2111 and -2221) showed strong inhibition of JSRV similar to that of wild type (WT) IFITM1, whereas chimeras containing the IFITM2 C terminus (IFITM1112 and -1222) were unable to restrict or enhanced JSRV infection (Fig. 1*D*). Notably, all of these chimeras exhibited similar inhibition of IAV infection (Fig. 1*D*). Western blotting showed that the expression levels of these constructs were similar to that of parental IFITM1 and -2 (Fig. 1*F*). Altogether, these results revealed that the C-terminal region of IFITM1 determines its different restriction of JSRV and IAV entry.

The most striking difference in the C-terminal region of IFITMs is the tail sequences downstream of the second putative membrane-spanning domain (MSD2); IFITM1 contains a relatively long tail, whereas IFITM2 terminates four residues after MSD2 (Fig. 1, *A–C*). The phenotypes of a series of C-terminal deletion mutants of IFITM1 confirmed a dominant role for the tail sequences, particularly residues 117–125, in the differential restriction of JSRV and IAV entry (Fig. 1, *E* and *G*).

The C-terminal Dibasic Residues Critically Control the Ubiquitination of IFITM1 but Differentially Modulate Viral Entry—We next focused on the potential motifs and residues within 117–125 (IIQEKRGY) that might modulate the cellular localization of IFITM1. We were particularly interested in tyrosine 125 (Tyr-125) and lysine (Lys-122) because these two residues are potentially phosphorylated and/or ubiquitinated (Fig. 1*A*). However, despite repeated attempts, we were unable to detect tyrosine phosphorylation of IFITM1 (data not shown) as we had previously shown for IFITM3 (22). Furthermore, replacement of Tyr-125 with phenylalanine or alanine (*i.e.* IFITM1 Y125F and Y125A) had no apparent effect on restriction of JSRV or IAV infection (Fig. 2, *A* and *B*), together suggesting that Tyr-125 is not critical.

We next examined whether the C-terminal Lys-122 residue of IFITM1 is ubiquitinated and its possible role in the antiviral effect. We found that IFITM1 WT can indeed be ubiquitinated; however, deletion of 112–125 or 117–125 substantially decreased the IFITM1 ubiquitination (Fig. 2*C*). Unexpectedly,

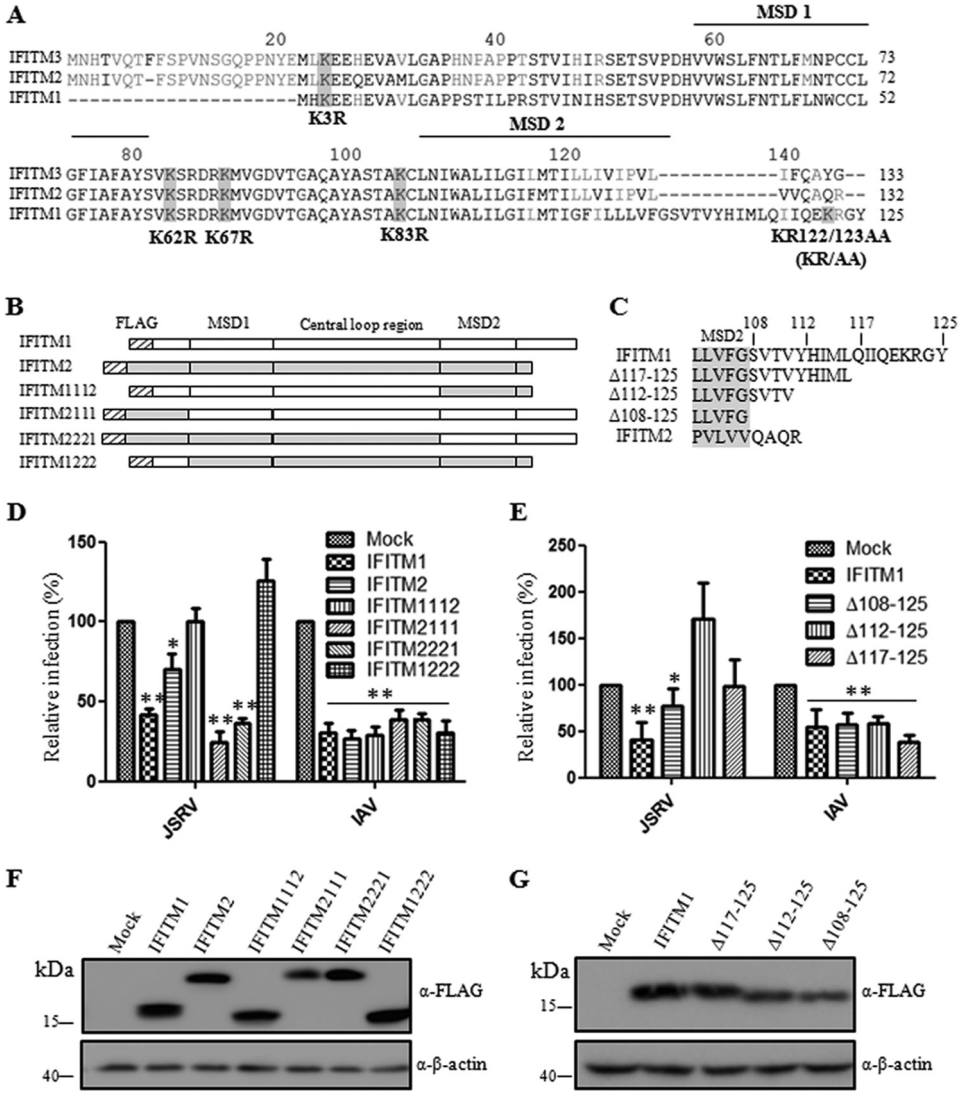

FIGURE 1. **The C terminus of IFITM1 modulates restriction of JSRV but not IAV entry.** *A*, alignment of human IFITM1, -2, and -3. The two putative membrane-spanning domains (MSD1 and MSD2) of IFITMs are indicated by *bars over* the alignment. Key point mutations used in this study are indicated. *B*, illustration of reciprocal chimeras between human IFITM1 (*white box*) and IFITM2 (*shaded box*). The N termini, two MSDs, central loop, and C-terminal sequences of IFITMs are delineated by *lines within* the *boxes*, whereas the FLAG epitope tag sequence is shown as a *hashed box*. *C*, sequences of the C-terminal deletion mutants of IFITM1 along with that of IFITM2 and parental IFITM1. *D* and *E*, relative infections of JSRV and IAV pseudovirions. A multiplicity of infection of 0.05–0.2 was typically used for infection. Infection was normalized to the level observed in HTX cells expressing empty vector (*Mock*). Values are the mean and S.E. (*error bars*) of 3–5 independent experiments. *, $p < 0.05$; **, $p < 0.01$. *F* and *G*, Western blotting analysis of the expression of chimeric (*F*) or C-terminal truncation mutants (*G*) using anti-FLAG antibody. β-actin serves as loading control.

we found that K122R, a mutant in which a double positive charge is preserved, still exhibited extensive ubiquitination, yet ubiquitination of IFITM1 was significantly lost in K122A, R123A, and KR/AA mutants (Fig. 2*D*). When all four conserved lysines were replaced by arginine (4KR), IFITM1 ubiquitination was still robust; however, combination of 4KR with KR/AA (4KR + KR/AA) resulted in an almost complete loss of IFITM1 ubiquitination (Fig. 2*D*). These results suggest that the positively charged KR residues are critical for IFITM1 ubiquitination, although the Lys-122 itself is not a key site of ubiquitination. Noticeably, all three Lys-to-Ala mutants exhibited enhanced inhibition of JSRV infection but had no significant effect on IAV (Fig. 2, *A* and *B*). We also tested the KR/AA mutants for 10A1 MLV, which is known to be relatively refractory to IFITM1 inhibition, and we found that KR/AA and 4KR + KR/AA substantially inhibited its Env-mediated entry and cell-cell fusion (Fig. 2, *E* and *F*). Altogether, these results indicate that the C-terminal KR residues are essential for IFITM1 ubiquitination, loss of which correlates with increased restriction of JSRV and 10A1 MLV entry.

IFITM1 KR Mutants Accumulate within Multivesicular Bodies (MVBs), Where They Co-localize with JSRV Pseudoviral Particles—We probed the subcellular distributions of IFITM1 WT and KR mutant proteins and interrogated their possible relationships to antiviral activities. HTX cells stably expressing WT or mutant IFITM1 were transfected with plasmids encoding YFP-Rab5, RFP-CD63, and YFP-LAMP1, which served as markers of early endosomes, late endosomes/MVBs, and lysosome, respectively. Compared with WT IFITM1, the KR/AA and 4KR + KR/AA mutants showed no significant difference in association with the early endosomal marker Rab5 but an increase in co-localization with CD63 (~10%; $p < 0.05$) (Fig. 3,

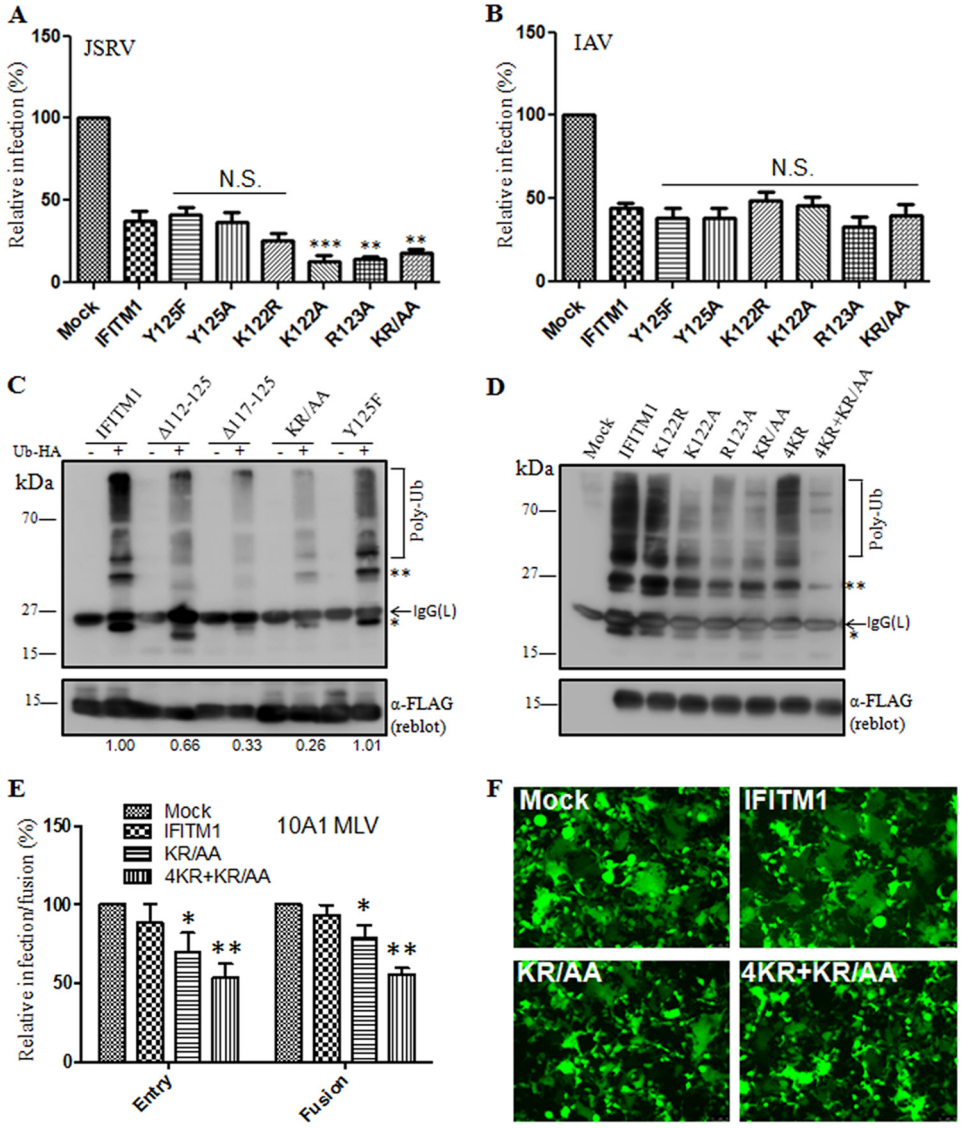

FIGURE 2. **The C-terminal dibasic residues of IFITM1 are critical for ubiquitination, and mutation of these residues results in reduced ubiquitination yet enhanced restriction of JSRV entry.** *A* and *B*, effect of the C-terminal IFITM1 mutation on JSRV and IAV pseudoviral infection. Values shown were normalized to the level of infection observed in mock expressing the empty vector and are the mean and S.E. (*error bars*) of 3–5 independent experiments. **, $p < 0.01$; ***, $p < 0.001$; *N.S.*, not significant. *C* and *D*, effect of the C-terminal deletion or point mutation of IFITM1 on ubiquitination. 293T cells were co-transfected with plasmids encoding the indicated IFITM1 and HA-tagged ubiquitin (*Ub-HA*). Cells were lysed, IFITM1 proteins were immunoprecipitated using anti-FLAG beads, and the ubiquitination pattern was detected by Western blotting using monoclonal anti-HA antibody (*top panels*). The same PVDF membrane was stripped, and IFITM1 proteins were detected by reblotting anti-FLAG monoclonal antibody (*bottom panels*). Single and double ubiquitination are indicated by *one* and *two asterisks*, respectively, and polyubiquitination is indicated on the *right* as *Poly-Ub*. The blots shown are representative of 3–4 independent experiments. *4KR*, an IFITM mutant with all four conserved lysines mutated to arginines (see Fig. 1*A*). *E* and *F*, effect of IFITM1 KR mutants on cell-cell fusion and entry mediated by 10A1 MLV Env. 293/LH2SN cells stably expressing the indicated IFITM1 proteins were co-transfected with 10A1 MLV Env with R peptide deleted and peGFP-N1 plasmid DNA. Values shown were normalized to that of parental cells (*Mock*) and are the mean and S.E. of three independent experiments. *, $p < 0.05$; ** $p < 0.01$.

A–*C*). In contrast, co-localization of the KR mutants with LAMP1 was decreased relative to WT IFITM1 (~20%; $p < 0.001$) (Fig. 3, *A* and *D*).

We then examined the co-localization of JSRV pseudovirions with RFP-CD63. MLV-Gag-YFP pseudovirions bearing JSRV Env were allowed to infect HTX cells expressing IFITM1 or KR/AA mutant, and cells were examined by deconvolution microscope. At 1 h postinfection, ~5–10% of JSRV pseudoviruses co-localized with RFP-CD63 (Fig. 4, *A* and *B*), consistent with their predominant localization on the plasma membrane, which reflected the relative slow entry process of JSRV (35, 36). At 4 h postinfection, a significant proportion of JSRV pseudovirus co-localized with CD63 (~50%, $p < 0.001$) (Fig. 4, *A* and *B*). We noticed that the overlap between Gag-YFP and RFP-CD63 was constantly lower for KR/AA as compared with IFITM1 WT at 4 h after infection, possibly due to the quantification method we used (*i.e.*, the fluorescence threshold-based rather than intensity-based assay). Nevertheless, these results indicate that the IFITM1 KR mutants accumulate in MVBs, where they co-localize with restricted JSRV pseudoviral particles.

IFITM1 Binds to AP-3, the Activity of Which Is Diminished When the C-terminal Dibasic Residues Are Altered—The cytoplasmic tails of many transmembrane proteins interact with the

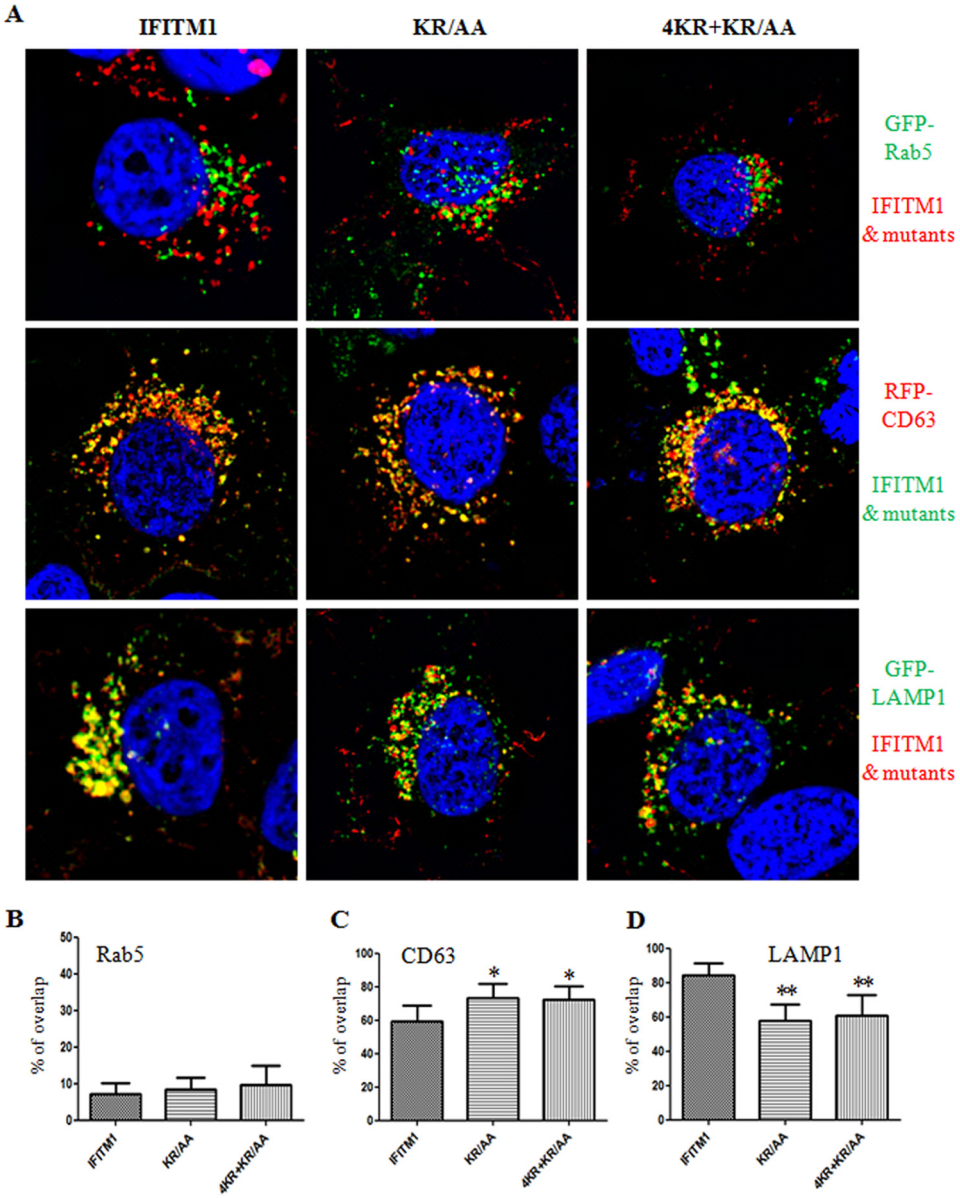

FIGURE 3. **Substitution of the dibasic KR residues of IFITM1 with alanines results in changes in protein subcellular distribution.** *A*, HTX cells stably expressing the WT or mutant IFITM1 were transfected with plasmids encoding GFP-Rab5, RFP-CD63, or GFP-LAMP1. Twenty-four hours after transfection, immunofluorescence staining was performed with anti-FLAG antibody to visualize IFITM1 proteins, and representative images were captured as described under "Experimental Procedures." Nuclei of cells were stained by DAPI. *B–D*, overlap quantification of WT or mutant IFITM1 proteins with the indicated markers (*i.e.* the percentage of IFITM1 proteins in host protein markers) was performed using National Institutes of Health ImageJ software based on ≥15 cells/sample. *, $p < 0.05$; **, $p < 0.01$. *Error bars*, S.E.

adaptor protein complexes (*i.e.* AP-1, AP-2, AP-3, AP-4, and AP-5) and thus are sorted into different intracellular compartments (37, 38). We therefore assessed the possible interactions of IFITM1 with the μ subunits of the adaptor protein complexes known to be essential for the sorting process. Among the four classical adaptor protein complexes tested, we found that IFITM1 strongly associated with the μ3A and μ3B subunits of AP-3 (Fig. 5*A*). A weak association between IFITM1 and the μ2 subunit of AP-2 was also observed, but none was detected for the μ subunits of AP-1 and AP-4 (Fig. 5*A*). Intriguingly, we found that K122A, R123A, KR/AA, and 4KR + KR/AA, but not K122R and 4KR, exhibited either a greatly decreased or complete loss of association with μ3A and μ3B (Fig. 5, *B* and *C*). These data revealed that IFITM1 protein specifically binds to AP-3 and, to a lesser extent, AP-2 and that the C-terminal dibasic residues are essential for this association.

Knockdown of AP-3 Modulates the Endocytic Trafficking and Antiviral Effect of IFITM1—We next tried to knock down AP-3 and examined its effect on antiviral activity. Five lentiviral shRNA clones purchased from Sigma (AP3M1, clones 098–102) were tested, and Western blotting revealed varied ability to decrease μ3A expression in transduced cells. Clones 098 and 100 showed the most potent knockdown efficiency (Fig. 6*A*) and were used in subsequent experiments. We found, interestingly, that knockdown of AP-3 itself substantially inhibited JSRV and 10A1 entry but had a modest effect on IAV (Fig. 6, *B–D*, compare the *first three columns*). Of note, expression of IFITM1 WT, but not the KR/AA mutant, in the AP-3 knock-

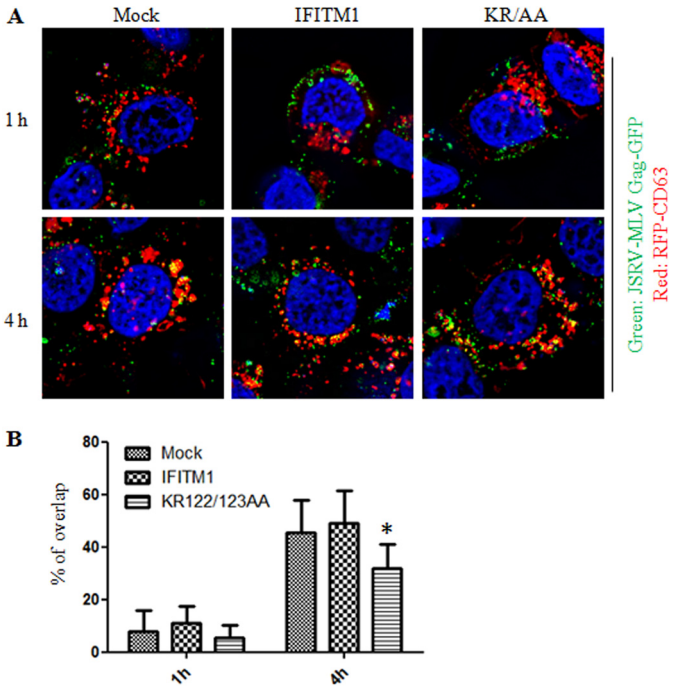

FIGURE 4. **JSRV pseudoviral particles co-localize with MVB marker CD63.** HTX cells stably expressing WT or mutant IFITM1 were transfected with a plasmid encoding RFP-CD63; cells were spinoculated with JSRV-MLV Gag-GFP pseudovirions at 4 °C for 2 h to allow virus binding to the cell. Cells were then washed twice with PBS to remove unbound viruses and switched to 37 °C. At the indicated time points, cells were imaged using deconvolution microscopy (*A*). Overlap quantification of JSRV pseudovirions with CD63 proteins was performed as described under "Experimental Procedures" (*B*). *, $p < 0.05$, indicating a difference between IFITM1 and KR/AA. *Error bars*, S.E.

down cells further enhanced inhibition of JSRV and 10A1 entry yet with no discernible effect on IAV (Fig. 6, *B–D*, compare the *second* and *last columns*). Flow cytometric analysis revealed that knockdown of AP-3 consistently, although not dramatically, increased the IFITM1 expression on the plasma membrane compared with that of shRNA-scrambled controls (Fig. 6*E*). This increase in IFITM1 expression by AP-3 knockdown mirrors our finding that the IFITM KR/AA mutant also exhibited an increased surface expression as compared with IFITM1 WT (data not shown). Immunostaining and three-dimensional deconvolution imaging analysis showed that IFITM1 exhibited an increased co-localization with CD63 yet a decreased co-localization with LAMP-1 in AP-3 knockdown cells, a phenotype that was similar to KR/AA (Fig. 3) (data not shown). Altogether, these results support a model in which the association of AP-3 with IFITM1 targets the protein to late endosomes and lysosomes, thus impairing its inhibition of JSRV and 10A1 that enter cells in an early endosome-related compartment or the plasma membrane.

IFITM1 Adopts More than One Membrane Topology Co-existing in Cellular Membranes—Our finding that the association of IFITM1 with cytosolic AP-3 depends on the C-terminal dibasic residues strongly argues that the C terminus of IFITM1 can be cytosolic, which is at odds with the originally proposed topology in which both terminal ends are extracellular or luminal (4). To directly address this issue, we interrogated the membrane topology of IFITM1 using SCAM (39). Specifically, cysteine residues were substituted for polar or charged residues located at the N terminus (S22C), central loop (R66C), second putative membrane-spanning domain (T97C), and C terminus (S108C and R123C) (Fig. 1*A*). We transfected 293T cells with these IFITM1 mutants and incubated cells with a membrane-impermeable reagent, mPEG (5 kDa), that labels unmodified cysteine residues with a polyethylene glycol chain of 5 kDa average mass. Retardation of migration by 5 kDa as detected by Western blotting would indicate that the cysteine residue of interest is labeled by mPEG and thereby exposed to the environment. The agent was applied to cells under three labeling conditions in parallel, each using exactly the same cell number: intact cells, cells whose plasma membrane was permeabilized by digitonin, and cells in which both the plasma and intracellular compartment membranes were permeabilized by Triton X-100.

In the absence of permeabilization, only segments present in the extracellular space can be labeled. Fig. 7*A* shows representative results of this analysis, and Fig. 7*B* summarizes the relative abundance of each species estimated from quantification of band intensities and normalized to the intensity seen in the non-permeabilized sample for each construct. We observed no increase in the mass of WT IFITM1 in non-permeabilized cells, indicating that the native Cys-50, Cys-51, and Cys-84 residues are not available for labeling (Fig. 7*A*, *left panels*; see Fig. 7*C* for the locations of these residues). The labeling of WT IFITM1 did not change when mPEG was given access to the cytosolic compartment (digitonin-permeabilized; Fig. 7*A*, *middle panels*); however, some labeling at a single cysteine occurred in Triton-permeabilized cells (Fig. 7*A*, *right panels*). These results imply that a small portion of WT IFITM1 contains only two palmitoylated cysteine residues, the third being unmodified and thus available for labeling. This interpretation is further supported by the small amounts of multiply pegylated ~30-kDa species detected for R66C and other IFITM1 mutant proteins in Triton-permeabilized cells (Fig. 7*A*, *right panels*), revealing that one natural cysteine residue (probably Cys-84) is labeled by mPEG under conditions in which plasma and intracellular compartment membranes are permeabilized.

Labeling of all cysteine mutants was greatest in samples from Triton-permeabilized cells, consistent with the preponderance of IFITM1 being in intracellular membranes (Fig. 7*A*, *right panels*). The bulk of IFITM1 S22C molecules presented their N terminus to the luminal and extracellular sides of membranes, whereas a relatively small portion of molecules oriented it into the cytosol, as evidenced by a modest increase in labeling of digitonin-permeabilized cells and a relatively larger increase in Triton-treated cells (Fig. 7, *A* and *B*). A small portion of molecules in the plasma membrane oriented their central loop toward the extracellular space, as evidenced by labeling of R66C in non-permeabilized cells (Fig. 7, *A* and *B*). However, this region was extensively exposed to the cytosol because labeling was substantially increased in digitonin-treated cells (Fig. 7, *A* and *B*). Similar to the central loop results, plasma membrane IFITM1 R123C was weakly labeled in non-permeabilized cells, supporting the idea that the C terminus can be oriented outside. Unexpectedly, no significant increase in labeling occurred in digitonin-permeabilized cells expressing R123C, indicating that few IFITM1 present their C terminus to the cytosol (Fig. 7,

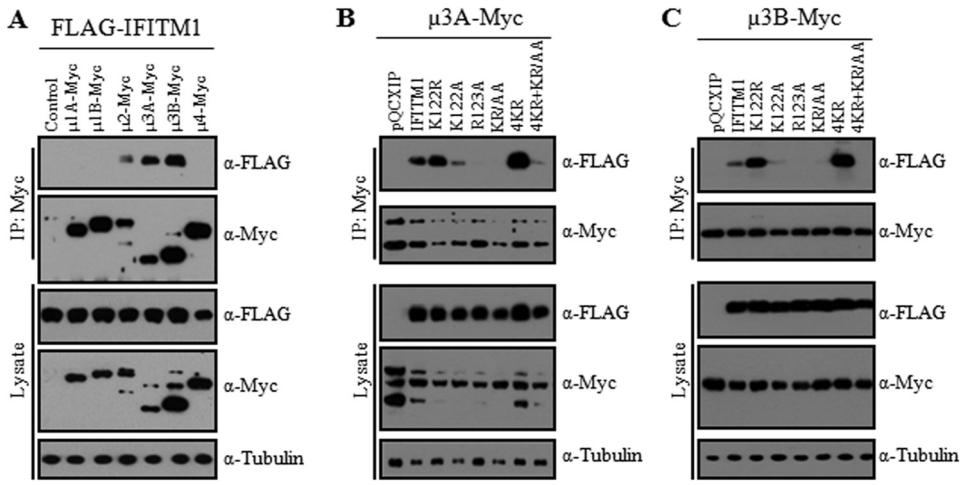

FIGURE 5. **IFITM1 binds to cellular AP-3s, an association that is lost when the dibasic residues are altered.** 293T cells were co-transfected with plasmids encoding FLAG-tagged WT or mutant IFITM1 as well as Myc-tagged μ subunits of adaptor protein complexes AP-1, AP-2, AP-3, and AP-4. Interacting complexes were identified by immunoprecipitation (*IP*) of cell lysates using anti-Myc antibody, followed by Western blotting using an anti-FLAG antibody to detect IFITM1. Input cell lysates were analyzed by direct blotting with an anti-Myc antibody; tubulin served as loading control.

A and *B*). Similar to the plasma membrane population of IFITM1 R123C, the intracellular R123C populations can present their C terminus on the luminal side, as evidenced by the large increase (7-fold) in labeling in Triton-treated cells (Fig. 7, *A* and *B*). We also tracked the membrane orientation of the C terminus using S108C. In this case, the cysteine residue lies adjacent to the end of the second membrane domain, a position that could have inhibited labeling by mPEG until cellular membranes are permeabilized by Triton X-100 (Fig. 7, *A* and *B*). A large increase in labeling under these conditions further supported the possibility that the C terminus is predominantly luminal. According to the estimates presented in Fig. 7*B*, we depicted the possible membrane topologies of IFITM1 that are probably present on the plasma membrane and in intracellular compartments (Fig. 7*C*; see "Discussion").

DISCUSSION

Compared with IFITM2 and -3, much less is known about how IFITM1 regulates its antiviral activity (2, 3). We showed in this study that replacing the dibasic motif of IFITM1 at the C terminus with alanines (KR/AA) increases inhibition of JSRV and 10A1 MLV but has no apparent effect on IAV. Whereas the KR to AA mutation caused a significant reduction in IFITM1 ubiquitination, the enhanced antiviral effect was not strictly correlated with the loss of IFITM1 ubiquitination. We interpret these results as implicating that the C-terminal KR*XX* motif is the dominant sorting motif that targets the IFITM1 protein to endolysosomal compartments, where different viruses fuse and enter host cells. Consistent with this notion, we showed that the KR mutants accumulate in MVBs, where JSRV pseudoviral particles are co-localized. However, because the KR*XX* motif is not conserved in mouse IFITM1 or in that of other species (5), the effect of the KR*XX* motif on viral entry may be human IFITM1-specific. In addition, other sorting signals, as yet to be discovered, may also be critical for the differential restriction of IFITM1 on viral infection.

Our discovery that human IFITM1 binds the cellular AP-3 protein complexes and that this activity is lost when the dibasic KR motif is replaced by alanine residues provides an interesting explanation as to how the C-terminal KR residues may influence IFITM1 endocytic trafficking and thus antiviral activities. Among the five adaptor protein complexes that are currently known to regulate sorting, endocytosis, and intracellular trafficking of transmembrane proteins, AP-3 is predominantly responsible for sorting transmembrane proteins from early endosomes to lysosome, the process of which can be clathrin-dependent or -independent (37). Consistent with this principle, we showed in this study that WT IFITM1 specifically associates with the μ3A and μ3B subunits of AP-3, and the IFITM1 protein is predominantly localized in lysosome. In contrast, the KR/AA mutants do not associate appreciably with AP-3 and exhibit increased accumulations in MVBs. In further support for a role of AP-3 in modulating IFITM1 antiviral effect, we showed that knockdown of AP-3 increases the inhibition of IFITM1 WT on JSRV and 10A1 entry, which has been shown to use the caveolar pathway for entry (36, 41), yet had no apparent effect on IFITM1 KA/AA mutant-mediated inhibition of viral entry. Interestingly, knockdown of AP-3 did not significantly affect IAV infection, suggesting that either the knockdown efficiency of AP-3 is not sufficient to influence IAV infection or, alternatively, IAV could use non-canonical pathways for infection (40). These results together suggest that the C-terminal KR residues of IFITM1 serve as an important sorting signal for AP-3 that probably targets the protein to late endosome and lysosome. The association of IFITM1 with AP-3, as well as its role in inhibiting viral infection, is in contrast to our recent report that IFITM3 specifically interacts with AP-2 via its Y*XX*θ-based motif (where θ represents a hydrophobic residue) and thus modulates restriction of viral entry (30).

Best known for Golgi to ER retrieval, interactions of the COP I sorting machinery with dibasic motifs have also been shown to be involved in membrane protein trafficking between the endosomal compartments (42). The classical dibasic motifs are C-terminal KK*XX* and K*X*K*XX* sequences, but there are examples of proteins retrieved using RK*XX* or K*X*H*XX* motifs (43).

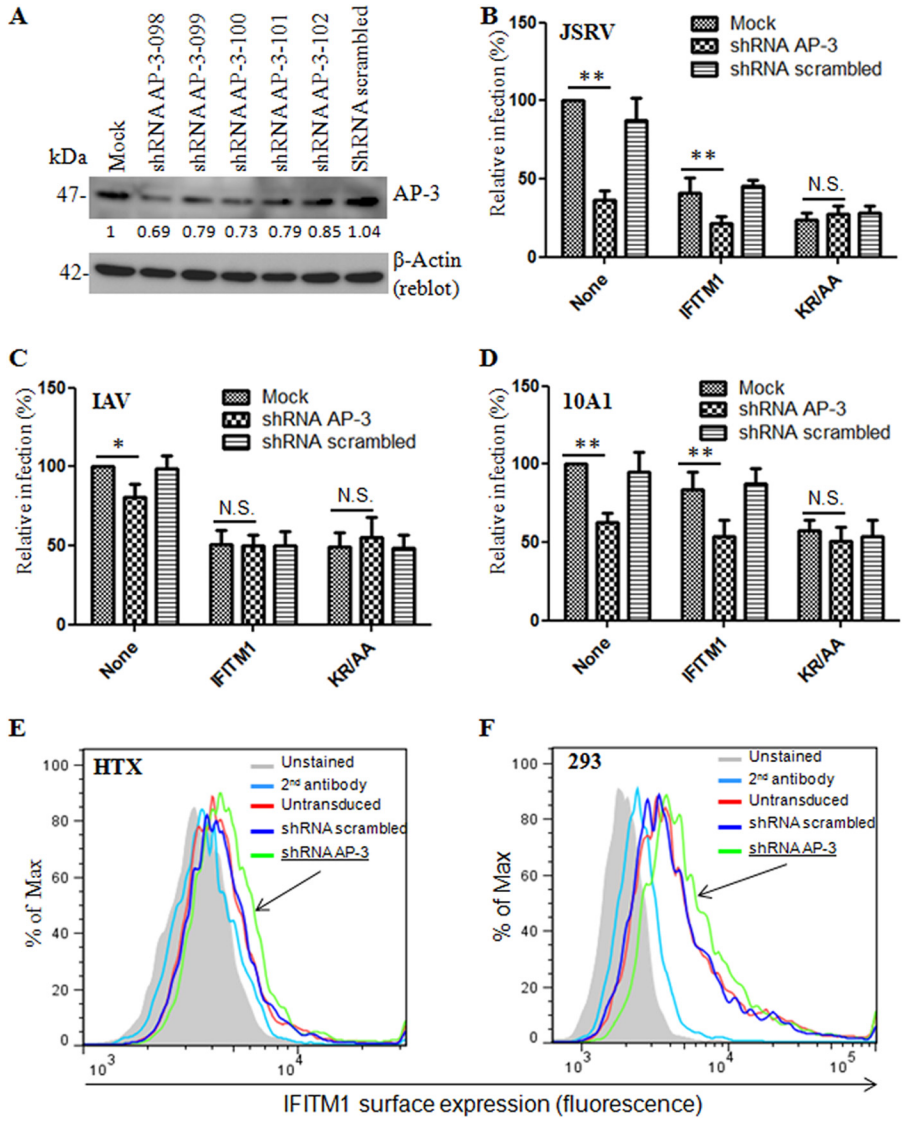

FIGURE 6. **Knockdown of AP-3 enhances the inhibitory effect of IFITM1 WT, but not the KR/AA mutant, on JSRV and 10A1 entry.** *A*, Western blotting analysis of HTX cells stably expressing lentiviral shRNA targeting AP-3 (μ3A) (five clones). The relative band intensity was quantified and indicated. The same PVDF membrane was reblotted with antibody against β-actin, which served as loading control. *B–D*, effect of AP-3 knockdown on JSRV, 10A1 MLV, and IAV entry. Parental HTX (*Mock*) or HTX cells stably expressing shRNA AP-3 (clone 098 or 100) or shRNA-scrambled were transduced by an empty pQCXIP vector (*None*) or pQCXIP vector expressing IFITM1 or KR/AA. Cells were infected with MLV pseudovirions bearing JSRV Env, 10A1 Env, or IAV HA/NA; the viral infection rates in parent HTX cells were set to 100% for comparison. Results represent the average ± S.D. (*error bars*) of 3–5 independent experiments. All comparisons were made between "mock" and "shRNA AP-3." *, $p < 0.05$; **, $p < 0.01$. *E* and *F*, effect of AP-3 knockdown on IFITM1 expression on the cell surface. HTX or 293 cells stably expressing IFITM1 were transduced or untransduced by lentiviral vectors expressing shRNA against AP-3 or scrambled shRNA; cells were examined for IFITM1 expression on the plasma membrane using anti-FLAG antibody by flow cytometry. Results represent one of the two independent experiments. *Unstained*, cells expressing IFITM1 were not incubated with any antibody. *2nd antibody*, cells expressing IFITM1 were only incubated with FITC-conjugated secondary antibody. *Untransduced*, cells expressing IFITM1 were not transduced by lentiviral shRNA but were incubated with both primary and secondary antibodies.

Although the C terminus of IFITM1 (KRGY, 122–125) is not canonical, two recent reports of the structure of a COP I complex bound to peptides showed that nearly canonical motifs can be recognized, albeit with lower affinities (43, 44). Specifically, the binding affinity for a KRLD-containing peptide was only 4-fold lower than for a canonical KKLD-containing peptide (43). This raises the possibility that evolution of a nearly canonical dibasic motif may provide a percentage of IFITM1 direct access to COP I-mediated sorting pathways in the endosomal compartments. Alternatively, in the absence of the dominant dibasic motif KRGY, a secondary sorting motif may become more active in determining sorting of the KR/AA mutant. Future experiments will determine the exact role of the C-terminal KR*XX* motif of IFITM1 in endosomal trafficking and to explore additional sorting motifs in this process.

Although there is general agreement that the highly conserved core sequences of IFITMs consist of two membrane-embedded domains separated by a central loop, their membrane topology is controversial (11, 20, 45). In this report, we provide the first biochemical evidence suggesting that IFITM1 exists in a mixed membrane topology in the cell. By quantifying the relative band intensity of mPEG-labeled IFITM1 mutants under two different permeabilization conditions and comparing them to labeling of non-permeabilized cells, we obtained

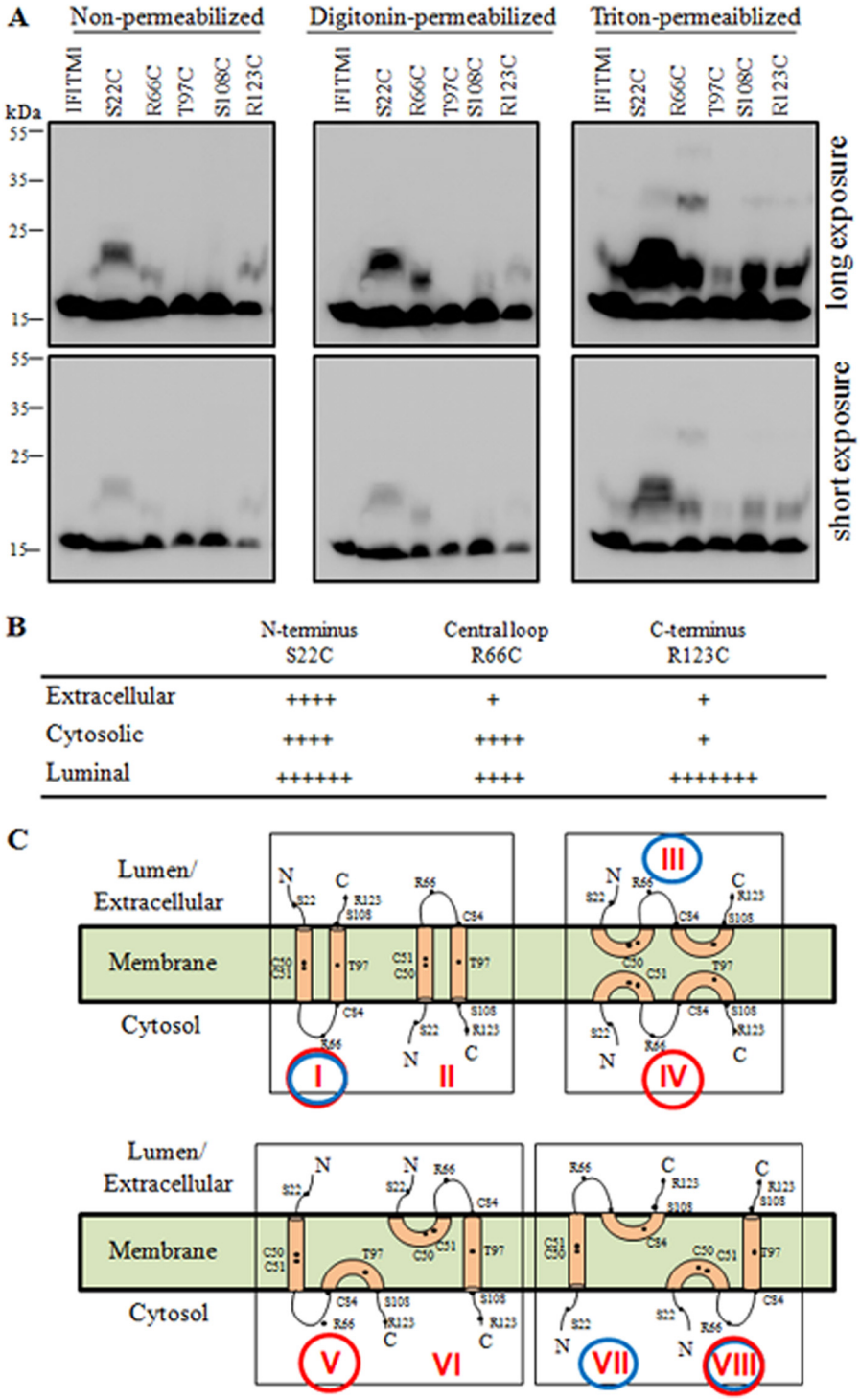

FIGURE 7. **IFITM1 adopts a mixed topology in cellular membranes determined by SCAM.** *A*, 293T cells were exposed to HCN buffer alone (non-permeabilized condition; *left panel*), digitonin (plasma membranes permeabilized; *middle panel*), or Triton X-100 (plasma and intracellular membranes permeabilized; *right panel*). Western blotting analysis was performed to detect the mPEG-labeled IFITM1 proteins using anti-FLAG antibody. Note that mPEG labeling of free-cysteine residues increases molecular mass by an average of 5 kDa. Residues in the N terminus (Ser-22), putative central loop (Arg-66), second putative membrane spanning domain (Thr-97), and C terminus (Ser-108 and Arg-123) were replaced with a cysteine residue for SCAM analysis. One representative experiment, with short and long exposure, is shown. The experiments were repeated more than five times, with similar patterns obtained. *B*, estimation of labeling signals of IFITM1 proteins under different permeabilization conditions. The band intensities were quantified by using Quantity One (Bio-Rad) and compared by setting the signal level of R66C and R123C under the non-permeabilization condition as "+". Note that the estimates shown are "net" signals (*i.e.* for "cytosolic," the signals of extracellular signals were deducted; for "luminal", the signals of both extracellular and cytosolic signals were subtracted). *C*, schematic diagrams of possible IFITM1 topologies deduced from Fig. 7*B*. The locations of cysteine-substituted residues are indicated. Each topology was assigned an arbitrary *Roman numeral* for ease of referral, with *red circles* indicating the predominant topology of IFITM1 on the plasma membrane (a combination of "extracellular" and "cytosolic") and the *blue circles* indicating the predominant topology of IFITM1 in intracellular compartments (a combination "luminal" and "cytosolic").

evidence that IFITM1 can adopt different membrane topologies co-existing as a mixture in cellular membranes (Fig. 7, *B* and *C*). Although the C terminus was labeled in non-permeabilized cells, its labeling did not significantly increase when the plasma membrane was permeabilized by digitonin (Fig. 7, *A* and *B*). This unexpected result indicated that only a small proportion of IFITM1 molecules adopt topologies in which the C terminus is cytosolic, which is consistent with a recent report (46). Another clue comes from the membrane orientations of the central loop and N terminus. Labeling of these two regions occurred in non-permeabilized cells (Fig. 7*A*), indicating that each can be oriented on the extracellular side of the plasma membrane. However, in contrast to the C terminus, labeling of the central loop and N terminus increased substantially after plasma membrane permeabilization with digitonin (Fig. 7, *A* and *B*), indicating that these regions also adopt a cytosolic orientation (Fig. 7*C*). Flow cytometry of non-permeabilized cells confirmed that in the plasma membrane the N and C terminus of IFITM1 can be presented to the extracellular space (data not shown) (5, 11). However, no apparent difference was observed between WT IFITM1 and its key KR/A mutants examined in this study (data not shown). Taken together, these results indicate that IFITM1 exists as a mixture of at least two topologies that share in common an extracellular/luminal orientation of the C terminus but differ in the orientations of their N terminus and central loop (Fig. 7*B*; see details below).

Based on the estimates presented in Fig. 7*B*, we depicted the possible membrane topologies for human IFITM1 protein (Fig. 7*C*). Among these, topologies I, IV, V, and VIII (*circled* in *red*) may be predominant on the plasma membrane, and topologies I, III, VII, and VIII (*circled* in *blue*), in which the C terminus is mainly luminal, are probably more abundant in intracellular vesicles. Given that the C terminus of IFITM1 is not significantly detected on the plasma membrane (Fig. 7, *A* and *B*), we interpret the data as implicating that IFITM1 is not predominantly present on the cell surface, consistent with the general notion that IFITMs, including IFITM1, primarily reside on endosomal compartments so as to inhibit pH-dependent virus entry (2, 3, 11). Of note, the different orientations of the central loop and N terminus need not necessarily occur in separate molecules (as between topology I and VII) but may occur within a set of molecules (as between topology III and VIII) or various combinations of these. Ultimately, it will be essential to understand how the different topologies of IFITM1 are controlled and related to membrane curvature and antiviral activities.

Acknowledgment—We thank Alexander Jurkevic (University of Missouri Molecular Cytology Core) for assistance in quantification of fluorescence images and colocalization analyses.

Note Added in Proof—Dr. Hong-Long Ji's contributions to this article fulfill the JBC authorship criteria but his authorship was inadvertently omitted from the version of the article that was published on December 17, 2014 as a Paper in Press.

REFERENCES

1. Sadler, A. J., and Williams, B. R. (2008) Interferon-inducible antiviral effectors. *Nat. Rev. Immunol.* **8,** 559–568
2. Diamond, M. S., and Farzan, M. (2013) The broad-spectrum antiviral functions of IFIT and IFITM proteins. *Nat. Rev. Immunol.* **13,** 46–57
3. Perreira, J. M., Chin, C. R., Feeley, E. M., and Brass, A. L. (2013) IFITMs restrict the replication of multiple pathogenic viruses. *J. Mol. Biol.* **425,** 4937–4955
4. Siegrist, F., Ebeling, M., and Certa, U. (2011) The small interferon-induced transmembrane genes and proteins. *J. Interferon Cytokine Res.* **31,** 183–197
5. Brass, A. L., Huang, I. C., Benita, Y., John, S. P., Krishnan, M. N., Feeley, E. M., Ryan, B. J., Weyer, J. L., van der Weyden, L., Fikrig, E., Adams, D. J., Xavier, R. J., Farzan, M., and Elledge, S. J. (2009) The IFITM proteins mediate cellular resistance to influenza A H1N1 virus, West Nile virus, and dengue virus. *Cell* **139,** 1243–1254
6. Huang, I. C., Bailey, C. C., Weyer, J. L., Radoshitzky, S. R., Becker, M. M., Chiang, J. J., Brass, A. L., Ahmed, A. A., Chi, X., Dong, L., Longobardi, L. E., Boltz, D., Kuhn, J. H., Elledge, S. J., Bavari, S., Denison, M. R., Choe, H., and Farzan, M. (2011) Distinct patterns of IFITM-mediated restriction of filoviruses, SARS coronavirus, and influenza A virus. *PLoS Pathog.* **7,** e1001258
7. Weidner, J. M., Jiang, D., Pan, X. B., Chang, J., Block, T. M., and Guo, J. T. (2010) Interferon-induced cell membrane proteins, IFITM3 and tetherin, inhibit vesicular stomatitis virus infection via distinct mechanisms. *J. Virol.* **84,** 12646–12657
8. Lu, J., Pan, Q., Rong, L., He, W., Liu, S.-L., and Liang, C. (2011) The IFITM proteins inihibit HIV-1 infection. *J. Virol.* **85,** 2126–2137
9. Chutiwitoonchai, N., Hiyoshi, M., Hiyoshi-Yoshidomi, Y., Hashimoto, M., Tokunaga, K., and Suzu, S. (2013) Characteristics of IFITM, the newly identified IFN-inducible anti-HIV-1 family proteins. *Microbes Infect.* **15,** 280–290
10. Jiang, D., Weidner, J. M., Qing, M., Pan, X. B., Guo, H., Xu, C., Zhang, X., Birk, A., Chang, J., Shi, P. Y., Block, T. M., and Guo, J. T. (2010) Identification of five interferon-induced cellular proteins that inhibit West Nile virus and dengue virus infections. *J. Virol.* **84,** 8332–8341
11. Li, K., Markosyan, R. M., Zheng, Y.-M., Golfetto, O., Bungart, B., Li, M., Ding, S., Liang, C., He, Y., Lee, J. C., Gratton, E., Cohen, F. S., and Liu, S.-L. (2013) IFITM proteins restrict viral membrane hemifusion. *PLoS Pathog.* **9,** e1003124
12. Mudhasani, R., Tran, J. P., Retterer, C., Radoshitzky, S. R., Kota, K. P., Altamura, L. A., Smith, J. M., Packard, B. Z., Kuhn, J. H., Costantino, J., Garrison, A. R., Schmaljohn, C. S., Huang, I. C., Farzan, M., and Bavari, S. (2013) IFITM-2 and IFITM-3 but not IFITM-1 restrict Rift Valley fever virus. *J. Virol.* **87,** 8451–8464
13. Anafu, A. A., Bowen, C. H., Chin, C. R., Brass, A. L., and Holm, G. H. (2013) Interferon-inducible transmembrane protein 3 (IFITM3) restricts reovirus cell entry. *J. Biol. Chem.* **288,** 17261–17271
14. Everitt, A. R., Clare, S., Pertel, T., John, S. P., Wash, R. S., Smith, S. E., Chin, C. R., Feeley, E. M., Sims, J. S., Adams, D. J., Wise, H. M., Kane, L., Goulding, D., Digard, P., Anttila, V., Baillie, J. K., Walsh, T. S., Hume, D. A., Palotie, A., Xue, Y., Colonna, V., Tyler-Smith, C., Dunning, J., Gordon, S. B., GenISIS Investigators, MOSAIC Investigators, Smyth, R. L., Openshaw, P. J., Dougan, G., Brass, A. L., and Kellam, P. (2012) IFITM3 restricts the morbidity and mortality associated with influenza. *Nature* **484,** 519–523
15. Bailey, C. C., Huang, I. C., Kam, C., and Farzan, M. (2012) Ifitm3 limits the severity of acute influenza in mice. *PLoS Pathog.* **8,** e1002909
16. Williams, D. E., Wu, W. L., Grotefend, C. R., Radic, V., Chung, C., Chung, Y. H., Farzan, M., and Huang, I. C. (2014) IFITM3 polymorphism rs12252-C restricts influenza A viruses. *PLoS One* **9,** e110096
17. Mills, T. C., Rautanen, A., Elliott, K. S., Parks, T., Naranbhai, V., Ieven, M. M., Butler, C. C., Little, P., Verheij, T., Garrard, C. S., Hinds, C., Goossens, H., Chapman, S., and Hill, A. V. (2014) IFITM3 and susceptibility to respiratory viral infections in the community. *J. Infect. Dis.* **209,** 1028–1031
18. John, S. P., Chin, C. R., Perreira, J. M., Feeley, E. M., Aker, A. M., Savidis, G., Smith, S. E., Elia, A. E., Everitt, A. R., Vora, M., Pertel, T., Elledge, S. J., Kellam, P., and Brass, A. L. (2013) The CD225 domain of IFITM3 is required for both IFITM protein association and inhibition of influenza A virus and dengue virus replication. *J. Virol.* **87,** 7837–7852

19. Feeley, E. M., Sims, J. S., John, S. P., Chin, C. R., Pertel, T., Chen, L. M., Gaiha, G. D., Ryan, B. J., Donis, R. O., Elledge, S. J., and Brass, A. L. (2011) IFITM3 inhibits influenza A virus infection by preventing cytosolic entry. *PLoS Pathog.* **7,** e1002337
20. Yount, J. S., Karssemeijer, R. A., and Hang, H. C. (2012) *S*-Palmitoylation and ubiquitination differentially regulate interferon-induced transmembrane protein 3 (IFITM3)-mediated resistance to influenza virus. *J. Biol. Chem.* **287,** 19631–19641
21. Yount, J. S., Moltedo, B., Yang, Y. Y., Charron, G., Moran, T. M., López, C. B., and Hang, H. C. (2010) Palmitoylome profiling reveals *S*-palmitoylation-dependent antiviral activity of IFITM3. *Nat. Chem. Biol.* **6,** 610–614
22. Jia, R., Pan, Q., Ding, S., Rong, L., Liu, S.-L., Geng, Y., Qiao, W., and Liang, C. (2012) The N-terminal region of IFITM3 modulates its antiviral activity through regulating IFITM3 cellular location. *J. Virol.* **86,** 13697–13707
23. Amini-Bavil-Olyaee, S., Choi, Y. J., Lee, J. H., Shi, M., Huang, I. C., Farzan, M., and Jung, J. U. (2013) The antiviral effector IFITM3 disrupts intracellular cholesterol homeostasis to block viral entry. *Cell Host Microbe* **13,** 452–464
24. Lin, T. Y., Chin, C. R., Everitt, A. R., Clare, S., Perreira, J. M., Savidis, G., Aker, A. M., John, S. P., Sarlah, D., Carreira, E. M., Elledge, S. J., Kellam, P., and Brass, A. L. (2013) Amphotericin B increases influenza A virus infection by preventing IFITM3-mediated restriction. *Cell Rep.* **5,** 895–908
25. Desai, T. M., Marin, M., Chin, C. R., Savidis, G., Brass, A. L., and Melikyan, G. B. (2014) IFITM3 restricts influenza A virus entry by blocking the formation of fusion pores following virus-endosome hemifusion. *PLoS Pathog.* **10,** e1004048
26. Bhanja Chowdhury, J., Shrivastava, S., Steele, R., Di Bisceglie, A. M., Ray, R., and Ray, R. B. (2012) Hepatitis C virus infection modulates expression of interferon stimulatory gene IFITM1 by upregulating miR-130A. *J. Virol.* **86,** 10221–10225
27. Raychoudhuri, A., Shrivastava, S., Steele, R., Kim, H., Ray, R., and Ray, R. B. (2011) ISG56 and IFITM1 proteins inhibit hepatitis C virus replication. *J. Virol.* **85,** 12881–12889
28. Wilkins, C., Woodward, J., Lau, D. T., Barnes, A., Joyce, M., McFarlane, N., McKeating, J. A., Tyrrell, D. L., and Gale, M., Jr. (2013) IFITM1 is a tight junction protein that inhibits hepatitis C virus entry. *Hepatology* **57,** 461–469
29. Zhao, X., Guo, F., Liu, F., Cuconati, A., Chang, J., Block, T. M., and Guo, J. T. (2014) Interferon induction of IFITM proteins promotes infection by human coronavirus OC43. *Proc. Natl. Acad. Sci. U.S.A.* **111,** 6756–6761
30. Jia, R., Xu, F., Qian, J., Yao, Y., Miao, C., Zheng, Y. M., Liu, S. L., Guo, F., Geng, Y., Qiao, W., and Liang, C. (2014) Identification of an endocytic signal essential for the antiviral action of IFITM3. *Cell Microbiol.* **16,** 1080–1093
31. Côté, M., Zheng, Y. M., Albritton, L. M., and Liu, S.-L. (2008) Fusogenicity of Jaagsiekte sheep retrovirus envelope protein is dependent on low pH and is enhanced by cytoplasmic tail truncations. *J. Virol.* **82,** 2543–2554
32. Janaka, S. K., Gregory, D. A., and Johnson, M. C. (2013) Retrovirus glycoprotein functionality requires proper alignment of the ectodomain and the membrane proximal cytoplasmic tail. *J. Virol.* **87,** 12805–12813
33. Côté, M., Zheng, Y. M., Li, K., Xiang, S.-H., Albritton, L. M., and Liu, S.-L. (2012) Critical role of a leucine-valine change in the distinct low pH requirements for membrane fusion between two related retrovirus envelope. *J. Biol. Chem.* **287,** 7640–7651
34. Zhou, H., Ferraro, D., Zhao, J., Hussain, S., Shao, J., Trujillo, J., Netland, J., Gallagher, T., and Perlman, S. (2010) The N-terminal region of severe acute respiratory syndrome coronavirus protein 6 induces membrane rearrangement and enhances virus replication. *J. Virol.* **84,** 3542–3551
35. Côté, M., Kucharski, T. J., and Liu, S.-L. (2008) Enzootic nasal tumor virus envelope requires a very acidic pH for fusion activation and infection. *J. Virol.* **82,** 9023–9034
36. Bertrand, P., Côté, M., Zheng, Y. M., Albritton, L. M., and Liu, S.-L. (2008) Jaagsiekte sheep retrovirus utilizes a pH-dependent endocytosis pathway for entry. *J. Virol.* **82,** 2555–2559
37. Bonifacino, J. S., and Traub, L. M. (2003) Signals for sorting of transmembrane proteins to endosomes and lysosomes. *Annu. Rev. Biochem.* **72,** 395–447
38. Hirst, J., Barlow, L. D., Francisco, G. C., Sahlender, D. A., Seaman, M. N., Dacks, J. B., and Robinson, M. S. (2011) The fifth adaptor protein complex. *PLoS Biol.* **9,** e1001170
39. Bogdanov, M., Heacock, P. N., and Dowhan, W. (2010) Study of polytopic membrane protein topological organization as a function of membrane lipid composition. *Methods Mol. Biol.* **619,** 79–101
40. Marsh, M., and Helenius, A. (2006) Virus entry: open sesame. *Cell* **124,** 729–740
41. Beer, C., Andersen, D. S., Rojek, A., and Pedersen, L. (2005) Caveola-dependent endocytic entry of amphotropic murine leukemia virus. *J. Virol.* **79,** 10776–10787
42. Kreis, T. E., Lowe, M., and Pepperkok, R. (1995) COPs regulating membrane traffic. *Annu. Rev. Cell Dev. Biol.* **11,** 677–706
43. Ma, W., and Goldberg, J. (2013) Rules for the recognition of dilysine retrieval motifs by coatomer. *EMBO J.* **32,** 926–937
44. Jackson, L. P., Lewis, M., Kent, H. M., Edeling, M. A., Evans, P. R., Duden, R., and Owen, D. J. (2012) Molecular basis for recognition of dilysine trafficking motifs by COPI. *Dev. Cell* **23,** 1255–1262
45. Bailey, C. C., Kondur, H. R., Huang, I. C., and Farzan, M. (2013) Interferon-induced transmembrane protein 3 is a type II transmembrane protein. *J. Biol. Chem.* **288,** 32184–32193
46. Weston, S., Czieso, S., White, I. J., Smith, S. E., Kellam, P., and Marsh, M. (2014) A membrane topology model for human interferon inducible transmembrane protein 1. *PLoS One* **9,** e104341